National Physical Laboratory

NPL REPORT IR 23

Digital approaches to field neutron spectrometry

K A A Gamage, N P Hawkes and G C Taylor

SEPTEMBER 2010

Digital approaches to field neutron spectrometry

K A A Gamage, N P Hawkes and G C Taylor
Acoustics & Ionising Radiation Division

ABSTRACT

Miniature digitizing electronics have been coupled to a detector based on an organic liquid scintillator to form a digital neutron and gamma spectrometer. The digitizing electronics are physically small enough to be packaged with a detector to form an easily portable unit. The spectrometer was exposed to a selection of the well-characterised radiation fields available at NPL, and the performance of three different neutron / gamma discrimination algorithms were compared. The energy resolution of the system was also assessed. Conclusions are presented on the best algorithm to use in such a system, and on the performance and ease of use of the spectrometer in comparison with conventional analogue systems.

ISSN 1754-2952

National Physical Laboratory
Hampton Road, Teddington, Middlesex, TW11 0LW

Approved on behalf of NPLML by Bajram Zeqiri, Knowledge Leader, Acoustics & Ionising Radiation Division.

Contents

Figures

Tables

1 Introduction

Organic liquid scintillators such as BC501A [1] or equivalents are a popular choice for neutron spectrometry at energies of around one to a few tens of MeV. This is because of their high efficiency, good resolution (compared with spectrometers such as Bonner spheres), and capacity for high count rates. However, they are sensitive to gammas as well as neutrons, and a means of discriminating between the two types of interaction is needed.

The scintillators have the property that neutron-induced pulses decay slightly more slowly than gamma-induced ones, allowing the shape of the pulse to be used as a basis for discrimination. This pulse shape discrimination (PSD) has been available for many years via specialised electronics (see Ref. [2] for example) or other techniques such as specially adapted photomultiplier bases [3].

Recently it has become possible to capture the entire pulse shape by means of fast digital sampling, enabling the power and flexibility of digital processing to be exploited. Experimenters are increasingly making use of this novel approach [4 - 7], and a variety of different algorithms have been proposed for carrying out the pulse shape discrimination (see below).

Up to now, most of the systems described in the literature have been based on rack-mounted electronic modules or on bulky instruments such as digital oscilloscopes. These are not ideal for portable (field) use, where the digitising electronics needs to be light, compact and with few controls. Miniature electronics meeting this need can now be constructed, but the sampling rate, amplitude resolution and / or processing power are likely to be restricted to some extent compared to the less portable devices, and it is not clear which of the various PSD algorithms would perform best in these circumstances.

The aim of the present work was to acquire data with a portable system in a number of different mixed neutron / gamma fields, and then analyse the data with a selection of algorithms, comparing the results on an equal footing. The relative complexities of the algorithms were also considered, bearing in mind that the portable spectrometer should ideally be able to analyse pulse shapes in real time, so as to transmit to the host laptop just the energy and type of the event. The energy resolution of the system was also assessed by reference to spectra from monoenergetic neutrons and gamma sources.

2 Digital spectrometer used in this study

The digitiser used in this study was the TOM board produced by Hybrid Instruments [8, 9]. This board measures 16 cm by 11 cm approximately, and is small enough to be packaged in the same housing as a detector if desired. The on-board ADC takes samples at up to 500 MHz, at an amplitude resolution of up to 12 bits (10.3 bits effective at maximum rate). A Virtex 5 FPGA controls the functions of the board and processes the data.

The FPGA normally executes an embedded analysis algorithm, but for the purposes of this project it was programmed to send raw pulse shapes to the host laptop using an Ethernet link. Each pulse shape consisted of 128 sample values taken at 2 ns intervals. A few pre-trigger samples were included, so that pulses from the detector typically reached maximum amplitude at sample number 26. The raw data included a substantial zero offset to allow for the input signal to change polarity; this has been subtracted for the analysis shown later in this report.

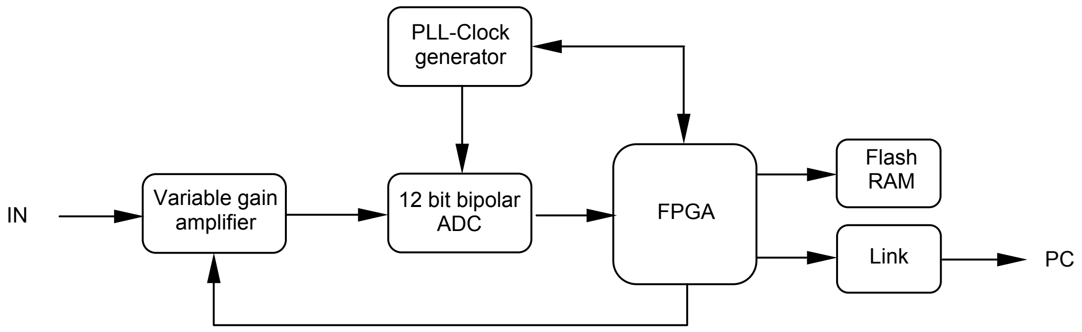

Figure 1. Schematic of TOM digitiser board.

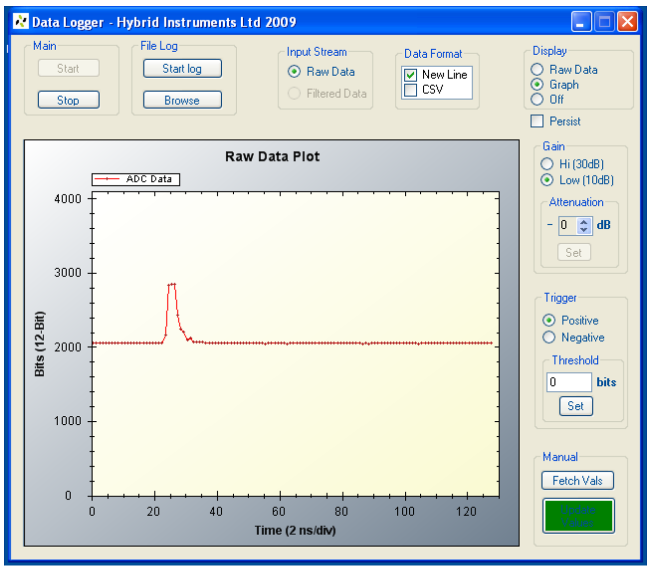

Figure 2. Screen image of software on host laptop.
The detector signal is actually negative-going, but is inverted by the software.
Sample values during a pulse are therefore predominantly positive
even after subtraction of the offset.

A schematic of the digitiser is given in Figure 1, and Figure 2 shows the control and monitoring interface of the data logging software on the host laptop. There are only three controls to adjust: the gain and attenuation of the analogue front end, and the setting of the trigger threshold.

The neutron / gamma detector consisted of a 6 cm diameter by 6 cm bubble-free cell containing BC501A, attached via a light guide to a Photonis XP2020 12-stage 51 mm diameter photomultiplier that was powered by a Photonis VD124K/T transistorised base.

Figure 3 shows all the components of the system except the HV unit, which was a conventional Tennelec 952 module. Two detectors appear in this Figure, but only the larger was used in this study.

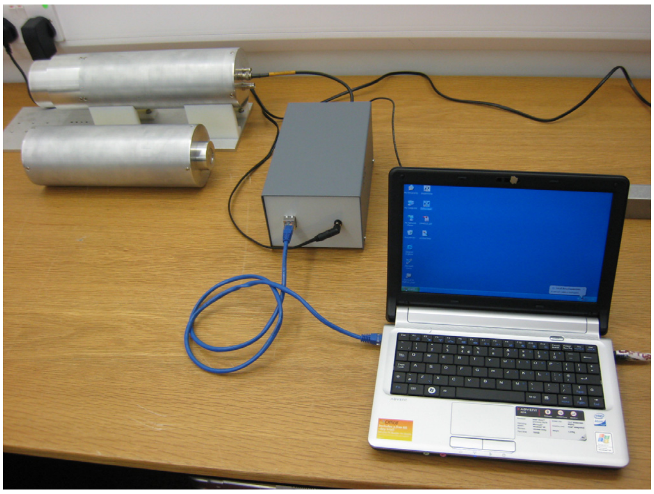

Figure 3. Digital spectrometer system.
For this study the digitiser was mounted in a separate metal housing (centre), but it is small enough to be incorporated with a detector if desired.

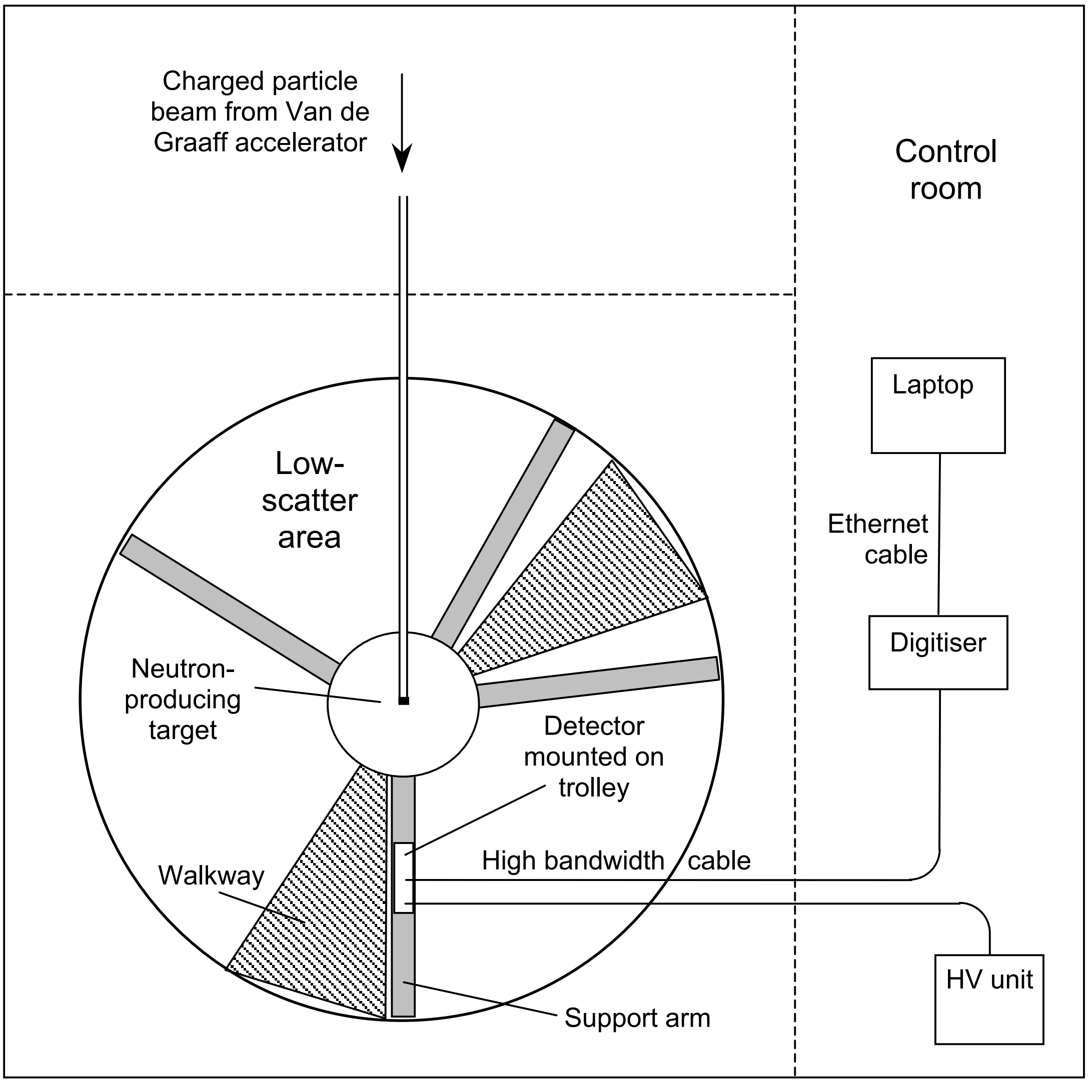

Figure 4. Typical experimental configuration.

3 Experimental method

The detector was exposed to three different sources of neutron / gamma radiation in turn: an ^{241}Am/Be source, 5 MeV monoenergetic neutrons, and a ^{252}Cf source.

The monoenergetic neutrons were generated by directing a deuteron beam from the NPL 3.5 MV Van de Graaff accelerator onto a thin TiD target at the centre of the low-scatter experimental area. The total beam charge delivered to the target was measured with a current integrator, which was calibrated in terms of neutron output by carrying out an additional experimental run with the NPL Long Counter (the efficiency of which is known) substituted for the digital spectrometer.

For the source-based measurements, the last two metres of the beam line were removed and the appropriate sealed source mounted near the detector.

A typical experimental configuration is shown in Figure 4. For most of the measurements the digitiser was located in the Control Room and connected to the anode of the detector using high bandwidth cable (Huber + Suhner SX07262BD) to preserve the pulse shape. This was convenient in case the customised data logging software on the laptop encountered a problem requiring the digitiser to be reset. However, measurements were also taken with the digitiser located in the experimental area and connected to the detector by a short length of RG58 cable, with approximately 40 m of Ethernet cable linking it to the laptop, and no difference in performance was observed.

For each measurement several tens of thousands of events were recorded, amounting to about 50 MB of data typically, and the data were then analysed off-line with each of three different pulse shape discrimination algorithms.

The energy resolution of the system was evaluated by reference to the light output spectrum of discriminated neutron events, derived from the 5 MeV monoenergetic data. A similar measurement was also made with a ^{22}Na gamma-only source.

4 Discrimination algorithms and Figure of Merit

Three algorithms, described below, were chosen for this project, and their performance evaluated in terms of a Figure of Merit (FoM) derived from the frequency distribution of the appropriate discrimination parameter. This distribution is expected to show two peaks, one corresponding to neutrons and the other to gammas, and the FoM was set equal to the separation of the peaks divided by the sum of their full widths at half maximum.

4.1 Charge comparison algorithm

In this approach the pulse is integrated over two different intervals ('long' and 'short'), and the ratio of the two integrals used as the discrimination parameter. The technique has been in use with analogue systems for many years (see Ref. [2]). In the present case, the long integral was always taken over the entire duration of the pulse. (In practice the sum of all the samples was used.) For the short integral, the aim was to capture just the tail of the pulse, which is larger in area for a neutron pulse than for a gamma pulse of the same total area. The best starting time was not obvious in advance, so the optimum value was found as described below. The end time of the short integral was fixed at the end of the pulse.

4.2 Pulse Gradient Analysis (PGA) algorithm

The PGA algorithm was described by D'Mellow et al. [10], and is based on measuring the amplitude of the pulse (the 'sample amplitude') a fixed time after the peak. The discrimination parameter used here is the ratio of the sample amplitude to the peak amplitude, which is larger for a neutron-induced pulse because of the longer decay time. The pulse is smoothed prior to processing, and in the present case a 15-point moving average was used, as mentioned by Joyce et al. [9]. The time interval between the peak and the second measurement was optimised as described below.

4.3 Model Pulse algorithm

Marrone et al. [4] describe a method in which a model neutron shape and a model gamma shape are derived by fitting a three-exponential model function to a set of known neutron and known gamma pulses. Unknown pulses are then characterised according to which of the two models they fit better, using a χ^2 criterion.

In the present case, the fitting process was found to be very dependent on the initial values used for the model parameters, making it impractical to carry out a large number of fits. Instead, the model pulses were derived by averaging a large number of known neutron and known gamma pulses. In this regard the method used here resembles the Fit to True Shape method described by Guerrero et al. [11]. 1704 neutron and 2990 gamma pulses (well separated under the Charge Comparison method) were extracted from the ^{241}Am/Be data set to construct the models (Figure 5).

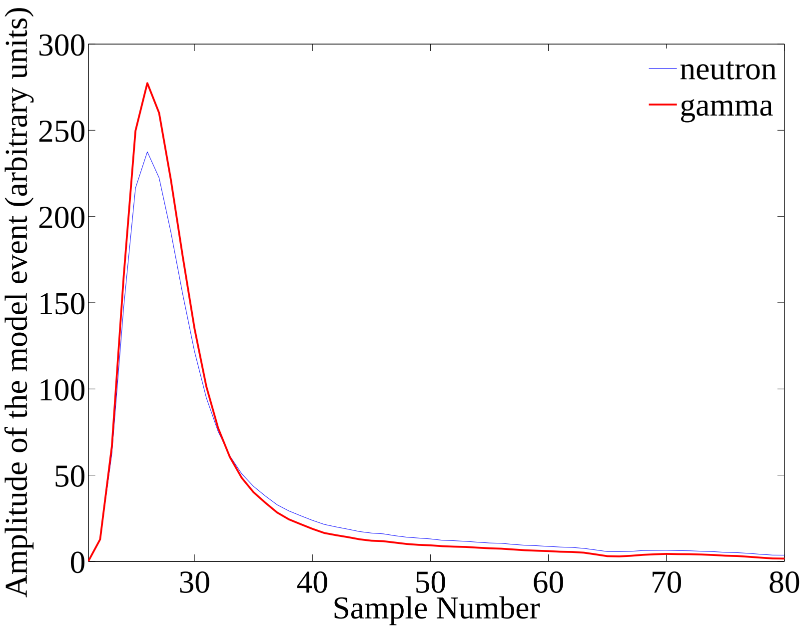

Figure 5. The model pulse shapes derived by averaging.

The averaging process resulted in some negative-going fluctuations at the beginning and end of the pulse. This problem was overcome by restricting the models to samples 21 - 80 only, as shown in the Figure. Points outside this range were not included in the χ^2 calculation.

Unknown pulses were characterised by calculating the difference between the χ^2 for the gamma model and that for the neutron model, scaling the area of the unknown pulse to that of the model first.

4.4 Amplitude limits

To prevent the FoM from being dominated by low energy events, and to avoid effects caused by an imperfectly sharp threshold, a lower limit was imposed on the total pulse area. Likewise an upper limit was imposed to exclude events where there was evidence of non-linearity in the digitiser. These limits are shown in Figure 6 for the ^{241}Am/Be data set. Only those events between the two dotted lines are used in the analysis. Different limits were allowed as appropriate for each data set (^{241}Am/Be, 5 MeV and ^{252}Cf), but for a given data set exactly the same events were used for all three algorithms.

5 Results

5.1 Discrimination quality and variation with light output

The ability of the algorithms to separate the events into neutron and gamma groups is illustrated in Figures 6 - 14 for all the datasets. Each point in these scatter plots represents one event, positioned according to two quantities arising from the algorithm in question. The quantities used for each algorithm are set out in Table 1. In each case, one of the quantities is a measure of the total size or area of the pulse, so the Figures in this Section show how the quality of the discrimination varies with the total light output of the event.

Table 1. Parameters used in scatter plots.

Algorithm	*X-axis quantity*	*Y-axis quantity*	*Neutron Group*	*Gamma Group*
Charge Comparison	Long integral*	Short integral	Upper branch	Lower branch
PGA	Sample amplitude	Peak amplitude*	Right branch	Left branch
Model Pulse	Total pulse area*	$\chi^2_\gamma - \chi^2_n$	Upper branch	Lower branch

*This quantity is a measure of the total light output.

For some algorithms, there was a parameter to be optimised (the short gate starting time for the Charge Comparison algorithm, and the peak-to-sample interval for PGA). This optimisation process is described in the next Section. The scatter plots in this Section are based on the optimised values.

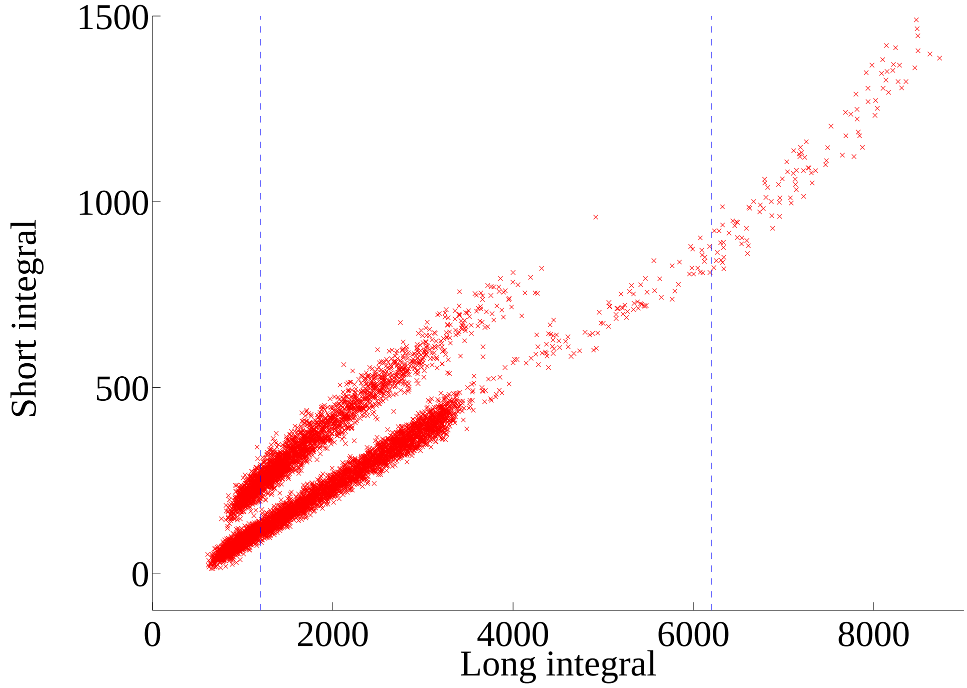

Figure 6. Analysis of the ^{241}Am/Be data with the Charge Comparison algorithm.
The dotted lines show the pulse amplitude limits; only those events lying between the lines are included in subsequent analysis. This same subset of events was used for all three algorithms.

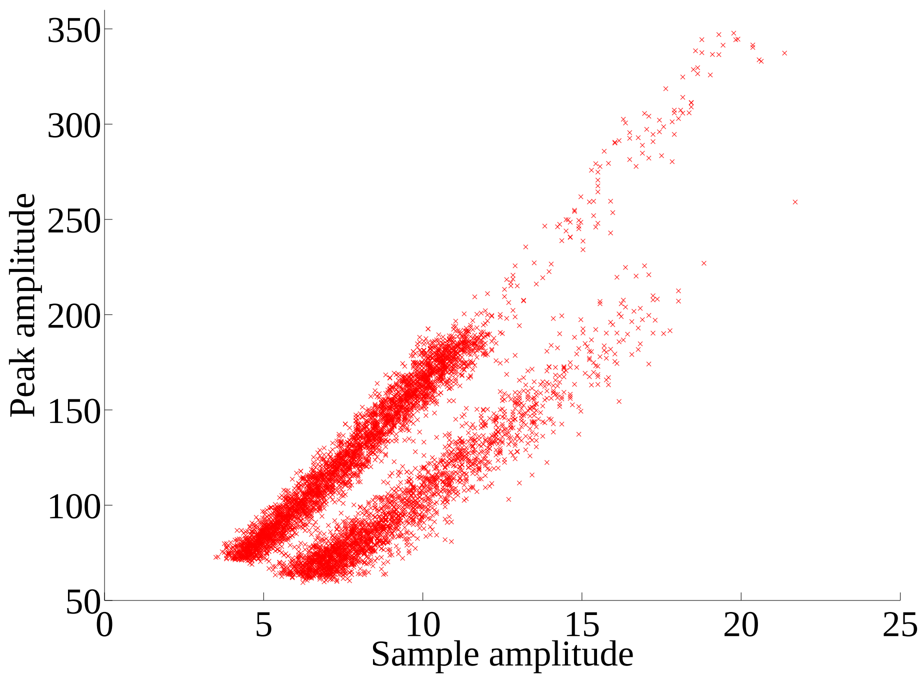

Figure 7. Analysis of the ^{241}Am/Be data with the PGA algorithm.
The amplitude values are in terms of the numbers returned by the digitiser.

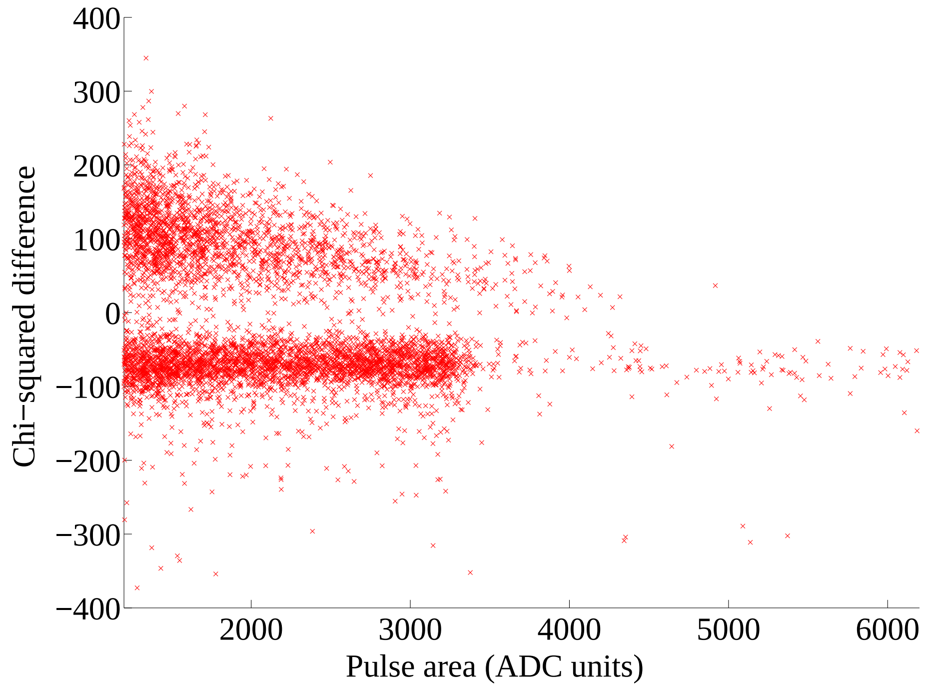

Figure 8. Analysis of the ^{241}Am/Be data with the Model Pulse algorithm.
The y-axis quantity is the difference between the χ^2 for the gamma model and that for the neutron model.

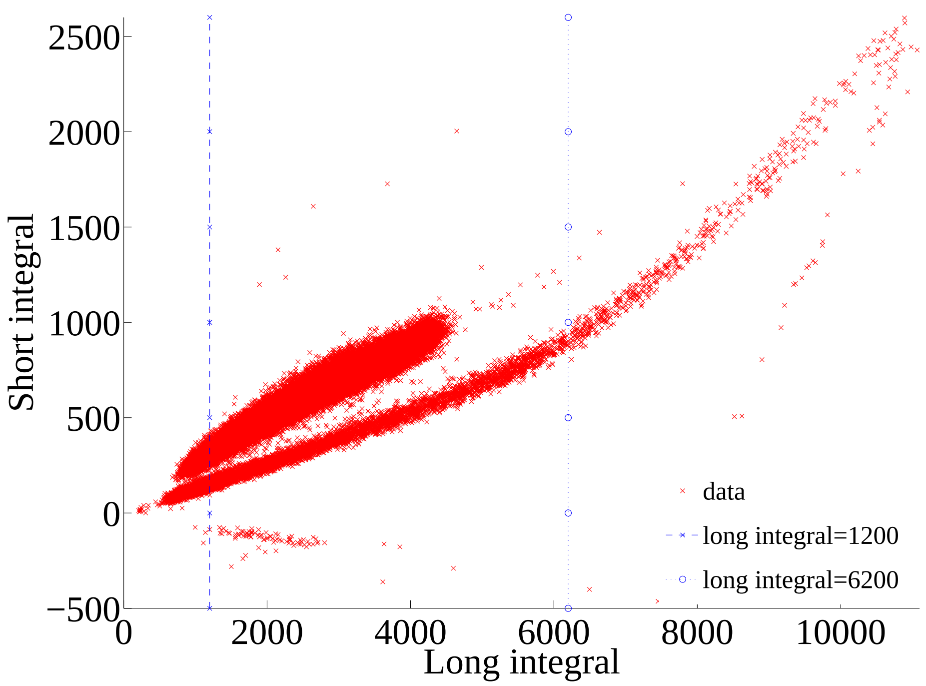

Figure 9. Analysis of the 5 MeV monoenergetic data with the Charge Comparison algorithm.
The vertical broken lines show the amplitude limits imposed for subsequent analysis. Again, the same subset of events was used for all three algorithms. The events outside the main branches are believed to be digitiser artefacts (see text below).

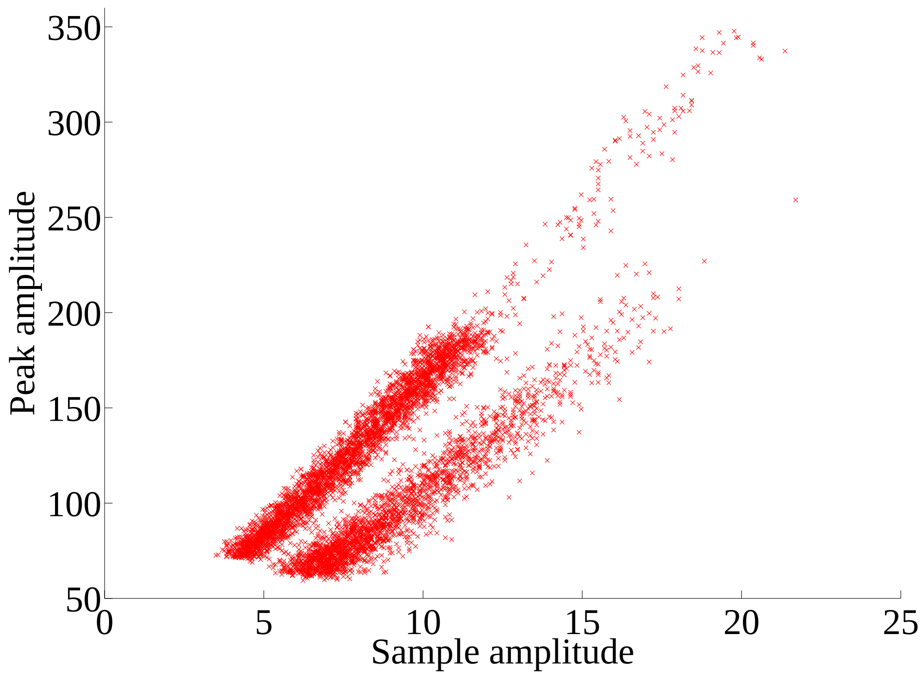

Figure 10. Analysis of the 5 MeV monoenergetic data with the PGA algorithm.

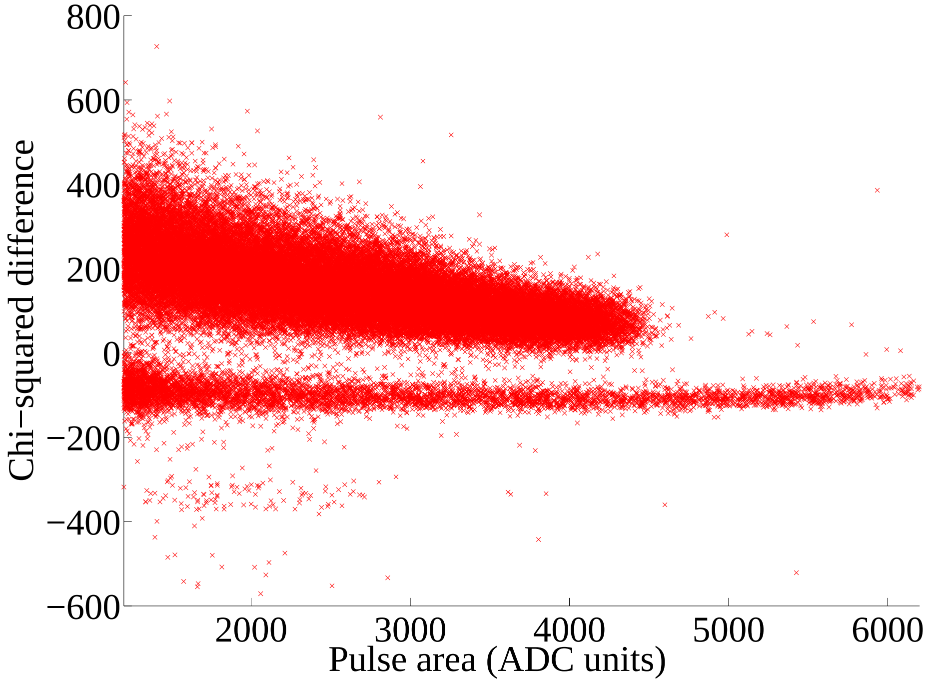

Figure 11. Analysis of the 5 MeV monoenergetic data with the Model Pulse algorithm.

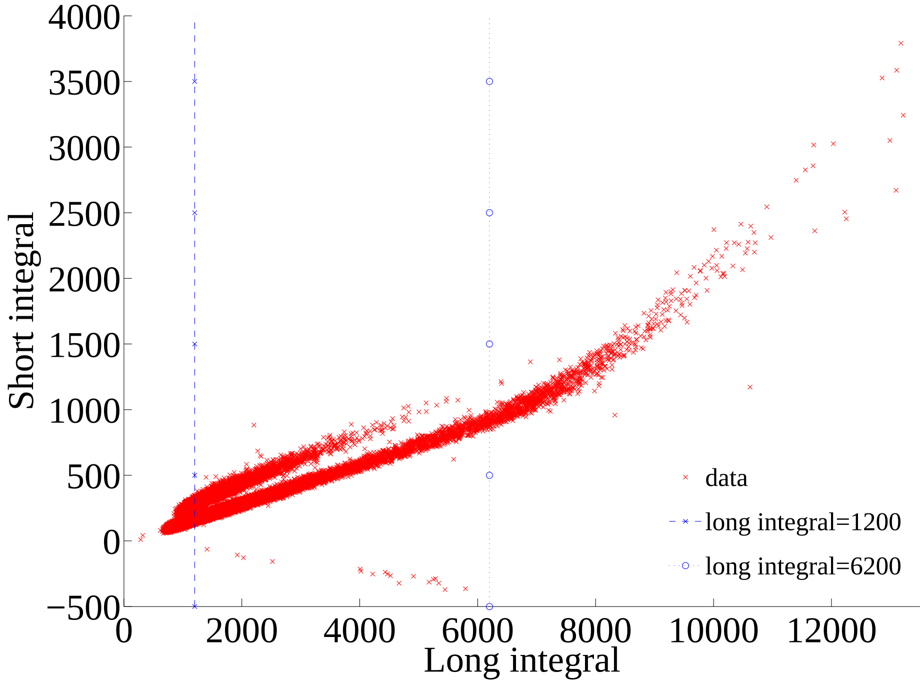

Figure 12. Analysis of the ^{252}Cf data with the Charge Comparison algorithm.
The vertical broken lines show the amplitude limits imposed for subsequent analysis.
The same subset of events was used for all three algorithms.

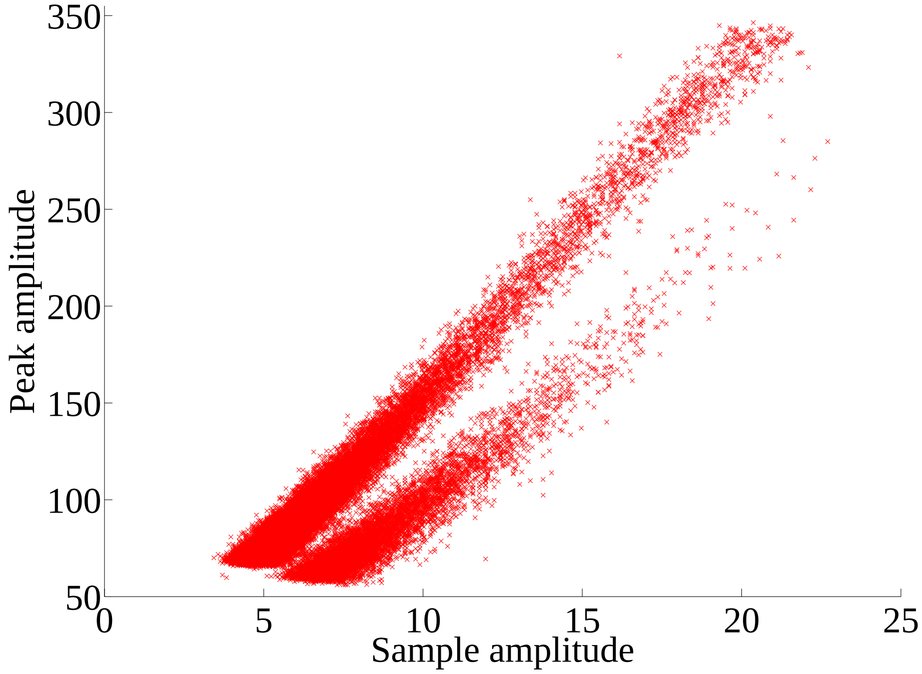

Figure 13. Analysis of the ^{252}Cf data with the PGA algorithm.

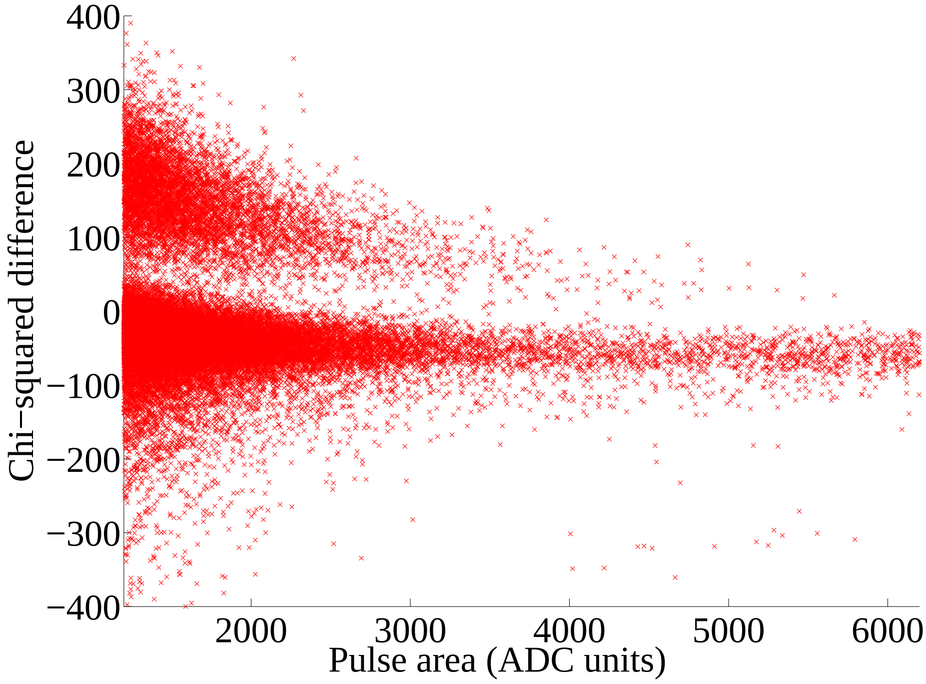

Figure 14. Analysis of the ^{252}Cf data with the Model Pulse algorithm.

The preceding Figures show that useable discrimination was achieved in all cases, the events clustering into two separate branches. The branch associated with the longer decay time is ascribed to neutrons and the other to gammas. The quality of the discrimination becomes poorer at low light outputs, with the neutron and gamma branches either becoming wider (in the Model Pulse algorithm), or drawing closer together (in the other algorithms).

The axis ranges of Figures 9 and 12 have been enlarged to show what appears to be the onset of non-linearity in the gamma branch. It is interesting that, beyond the curved region, the gamma branch appears to resume its linear behaviour but at a different gradient. The same Figures also show a small proportion of events that do not lie in either the neutron or gamma branches. These events appeared to occur in bursts and to be more prevalent when the digitiser gain was increased. The causes of these unexpected behaviours are unclear and are to be investigated further in later studies.

5.2 Optimisation of the FoM

To calculate a single FoM for the entire range of light outputs, the discrimination parameter used must be independent of light output. Table 2 shows the quantity used as the discrimination parameter for each algorithm.

The FoM was calculated by deriving the value of the discrimination parameter for each event in the data set, histograming these values, and then fitting Gaussians to the two peaks in the histogram. The FoM was set equal to the difference between the means of the Gaussians divided by the sum of their full widths at half maximum.

The Charge Comparison and PGA algorithms both have a quantity to be adjusted for best FoM, as set out in Table 2. This was done by plotting the FoM derived from the ^{241}Am/Be data set as a function of the value of the quantity. The optimum value was then chosen from this plot, with the aid of a polynomial fit to smooth out fluctuations in the FoM. Because of these fluctuations, the final optimised FoM for the algorithm was taken from the polynomial fit rather than from an individual FoM calculation.

Figures 15 and 16 show this process for the Charge Comparison and PGA algorithms respectively.

Table 2. Discrimination parameters and optimisation for each algorithm.

Algorithm	*Discrimination parameter*	*Adjusted quantity*	*Optimum value*
Charge Comparison	Ratio of short to long integrals	Short integral starting time	Sample #40 (14 samples or 28 ns after the peak)
PGA	Ratio of sample amplitude to peak amplitude	Time interval between peak and sample	24 digitiser sample intervals (48 ns)
Model Pulse	$\chi^2_\gamma - \chi^2_n$	None	

Once determined from the ^{241}Am/Be data set as described above, the value of the adjusted quantity was not changed for the other data sets. However, because of the substantial FoM fluctuations evident in Figures 15 and 16, it was decided to produce similar plots of FoM against adjusted quantity for the other data sets as well, even though the value was not to be changed, so that the final FoM for the algorithm could be taken from the polynomial fit. Figures 17 - 20 show these plots.

For the Model Pulse algorithm, there was no quantity to optimise, and the FoM was calculated only once for each data set.

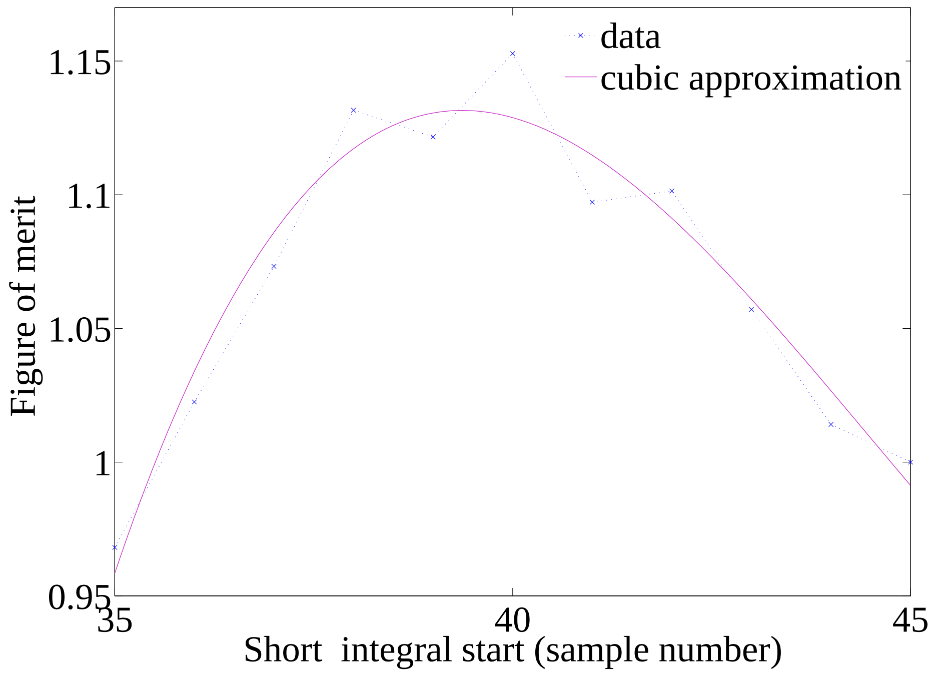

Figure 15. Optimisation of Charge Comparison algorithm using ^{241}Am/Be data.

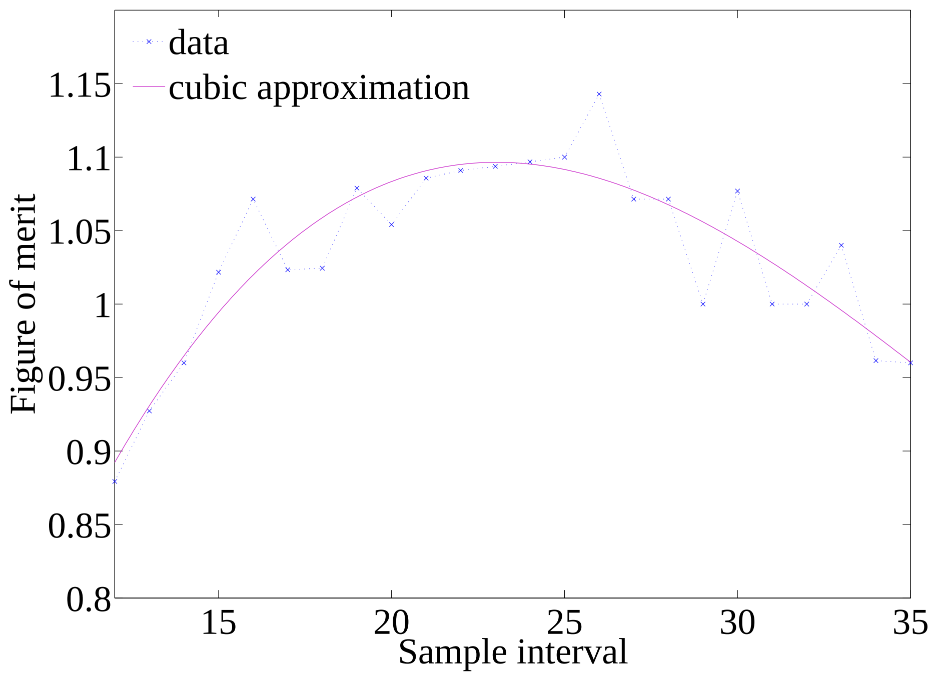

Figure 16. Optimisation of the PGA algorithm using ^{241}Am/Be data.

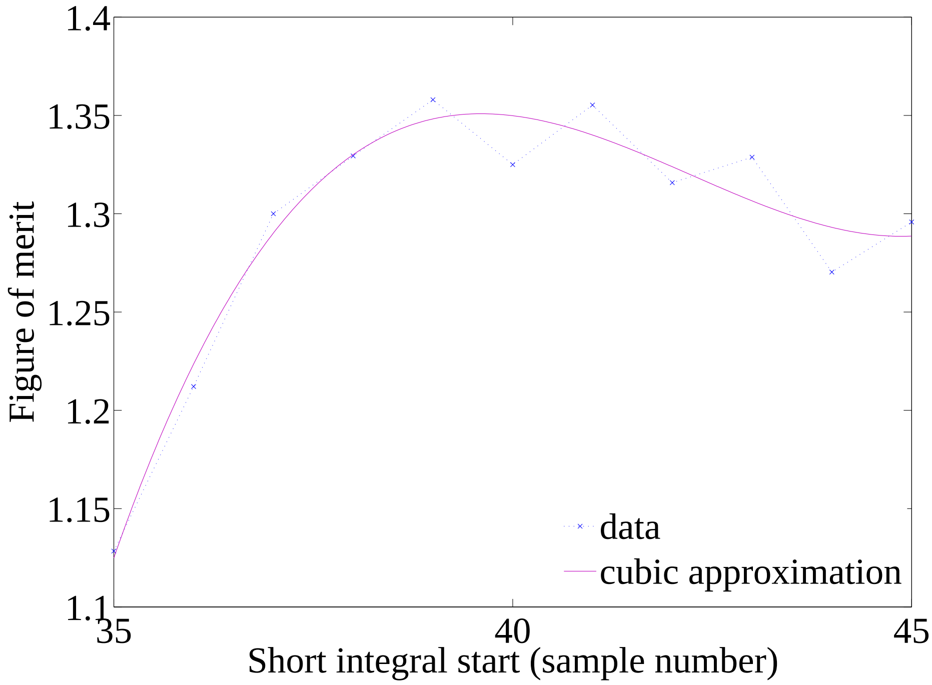

Figure 17. FoM determination for Charge Comparison algorithm with 5 MeV data.

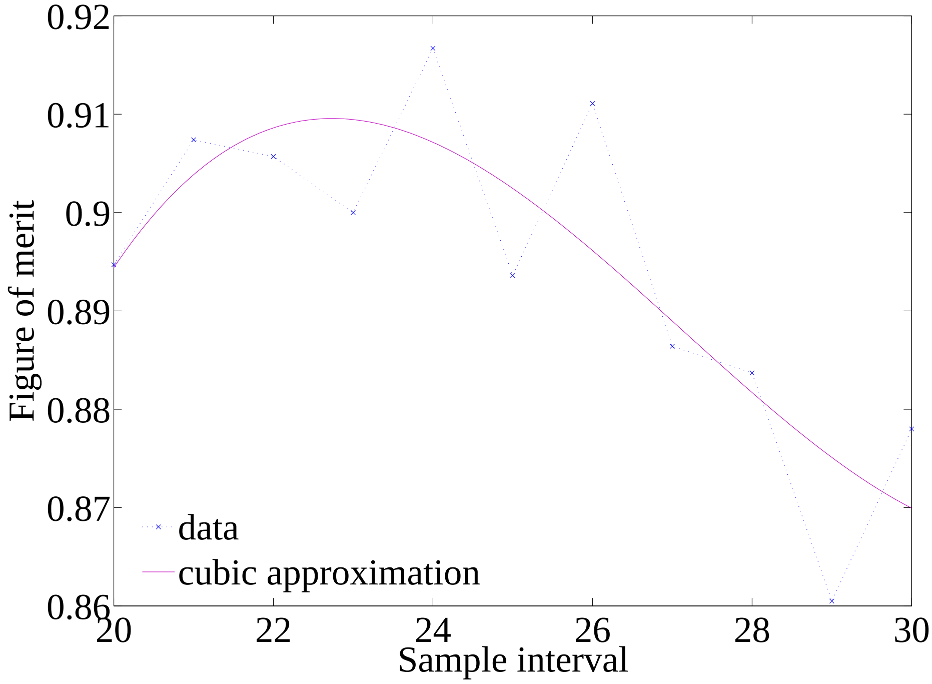

Figure 18. FoM determination for PGA algorithm with 5 MeV data.

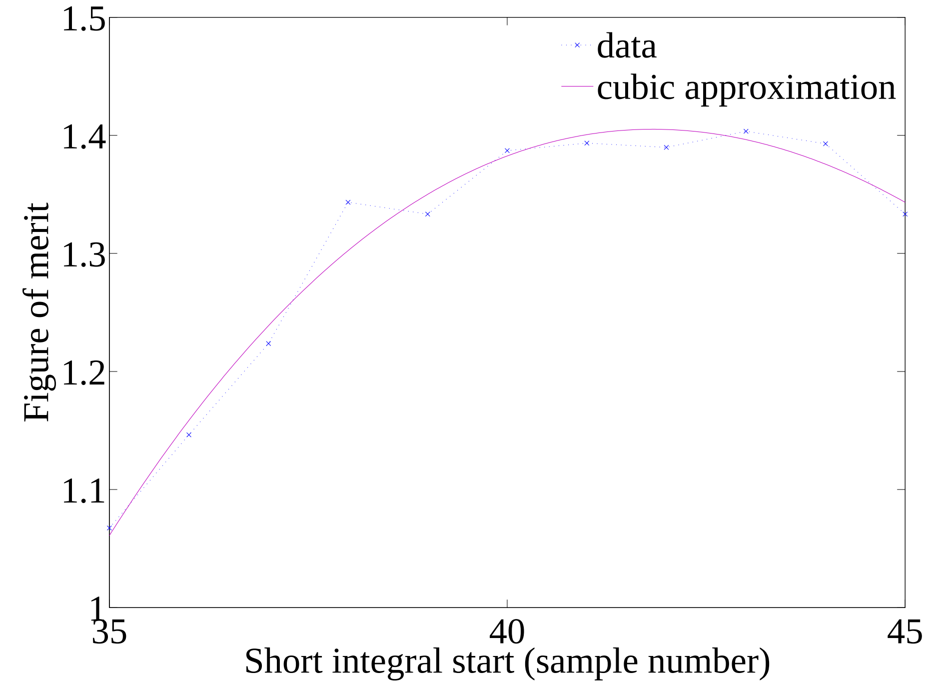

Figure 19. FoM determination for Charge Comparison algorithm with ^{252}Cf data.

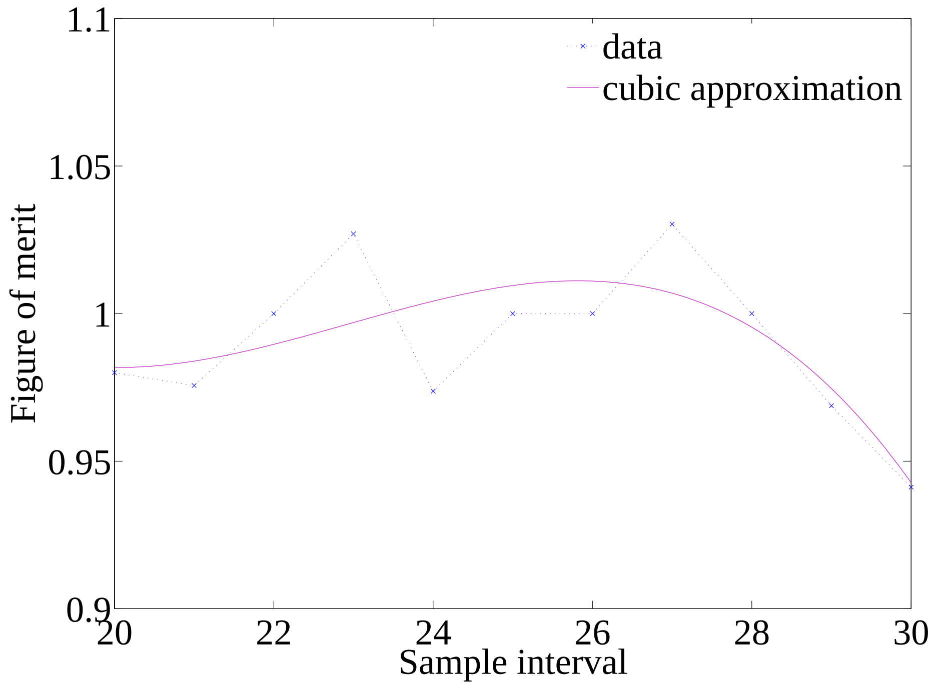

Figure 20. FoM determination for PGA algorithm with ^{252}Cf data.

5.3 FoM histograms

Figures 21 - 29 show the discrimination parameter histograms from which the FoM values were derived, including the fitted Gaussians. They correspond to the optimised value of the adjusted quantity, where applicable.

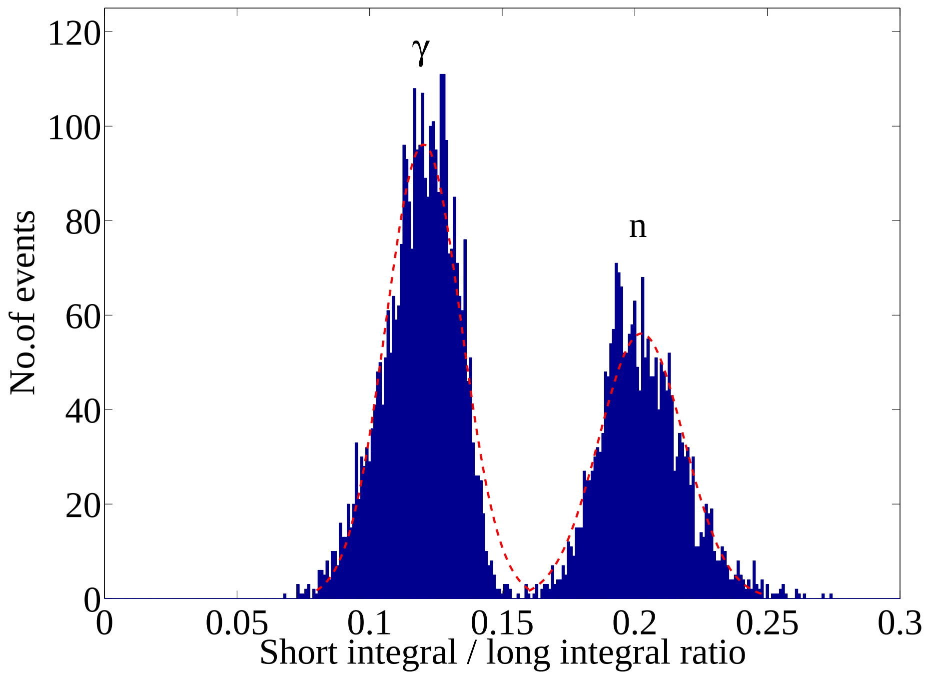

Figure 21. FoM histogram for Charge Comparison algorithm with ^{241}Am/Be data.

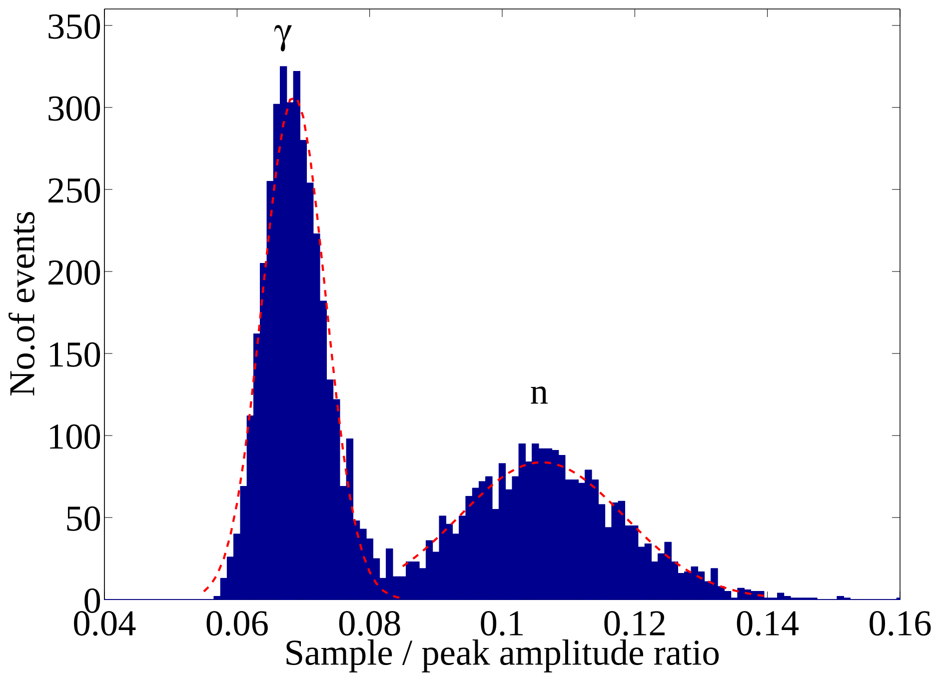

Figure 22. FoM histogram for PGA algorithm with ^{241}Am/Be data.

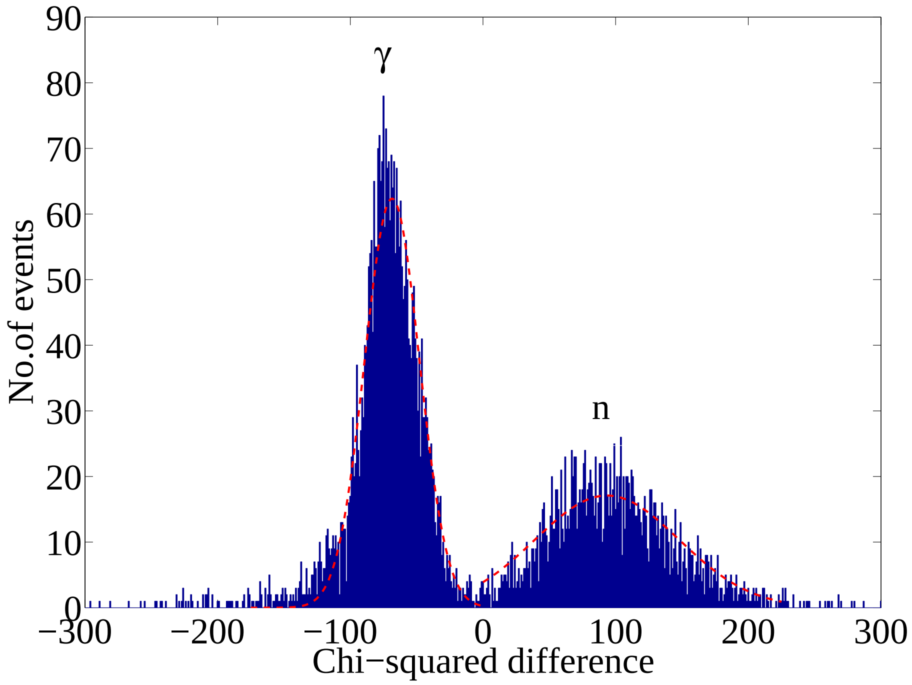

Figure 23. FoM histogram for Model Pulse algorithm with ^{241}Am/Be data.

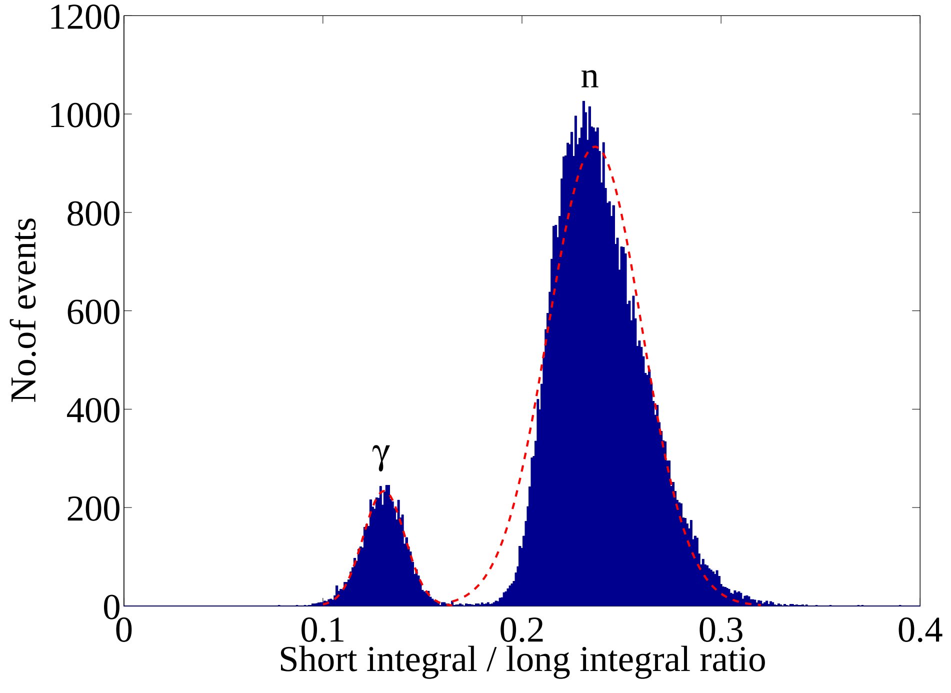

Figure 24. FoM histogram for Charge Comparison algorithm with 5 MeV data.

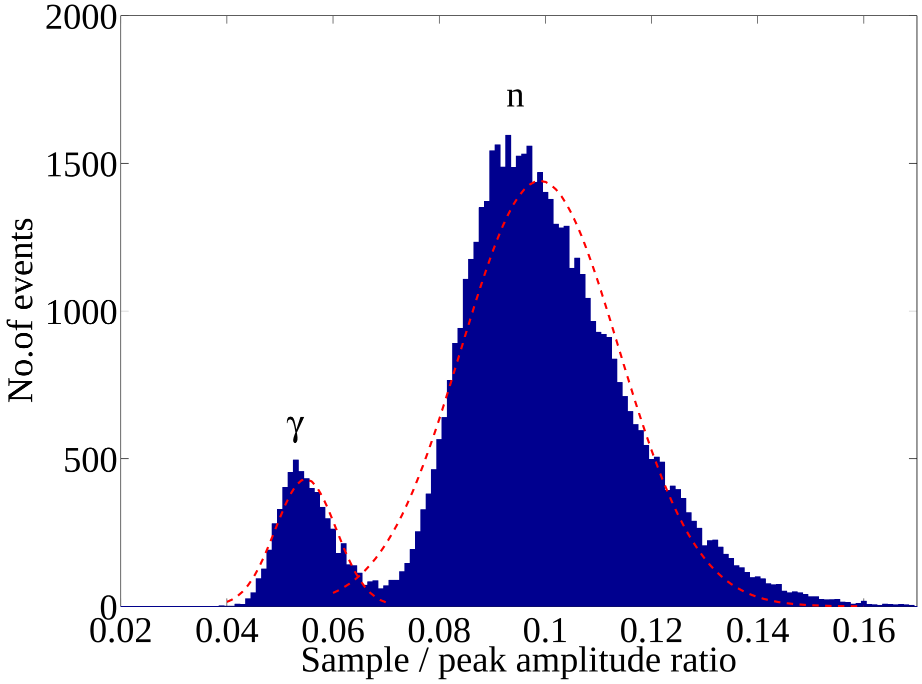

Figure 25. FoM histogram for PGA algorithm with 5 MeV data.

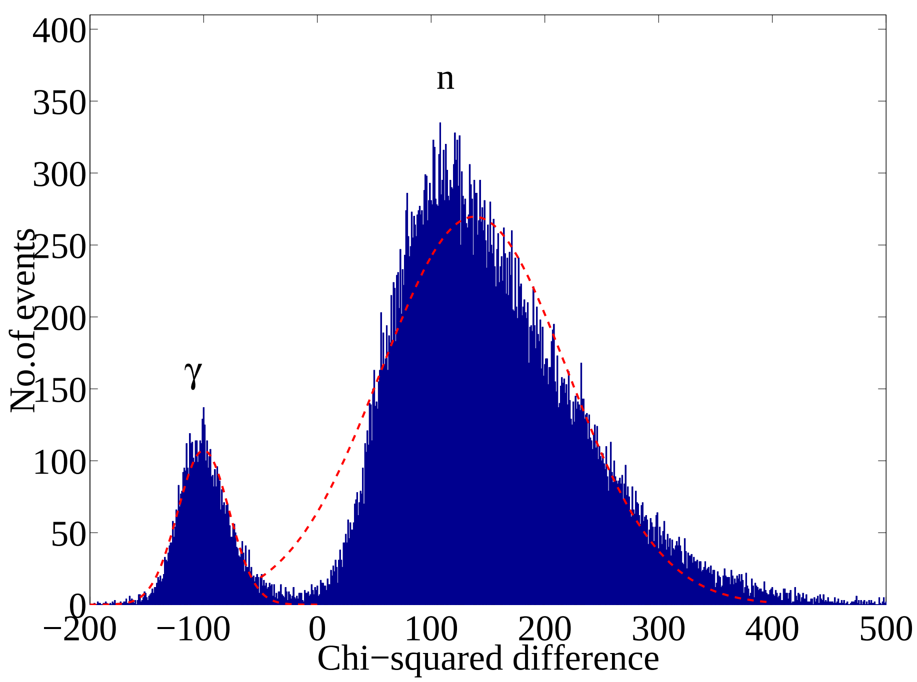

Figure 26. FoM histogram for Model Pulse algorithm with 5 MeV data.

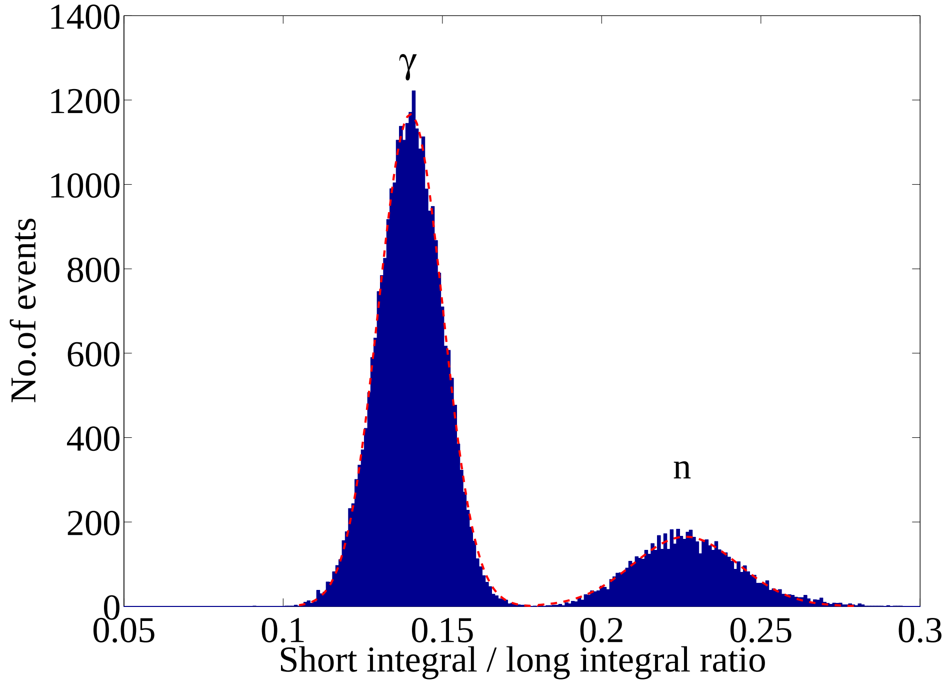

Figure 27. FoM histogram for Charge Comparison algorithm with ^{252}Cf data.

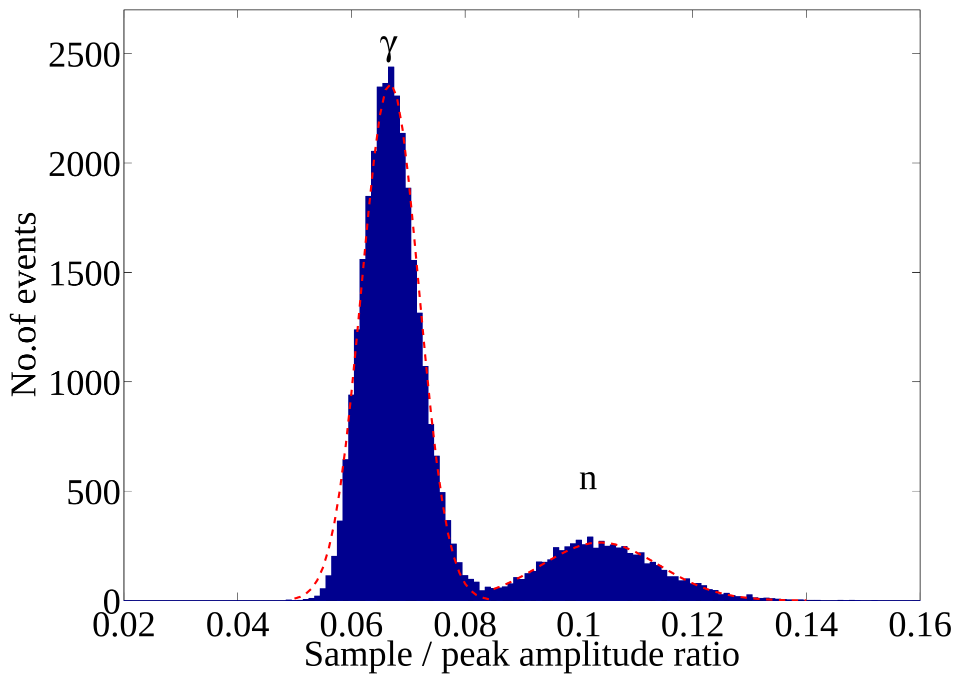

Figure 28. FoM histogram for PGA algorithm with ^{252}Cf data.

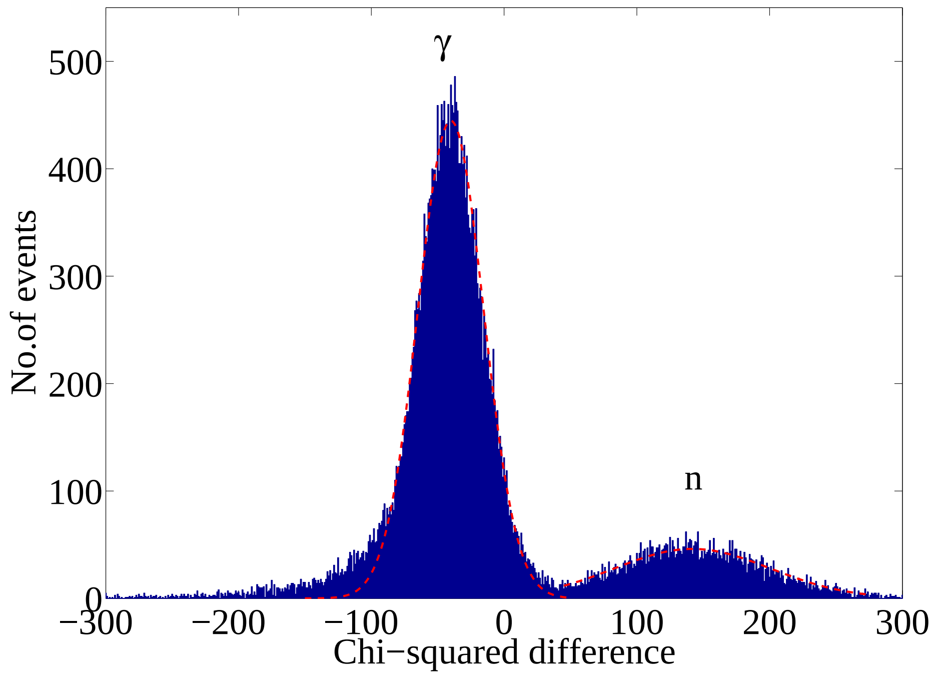

Figure 29. FoM histogram for Model Pulse algorithm with ^{252}Cf data.

It is interesting that, for a given data set, the three algorithms produce similar histograms, despite their different approaches to the calculation.

5.4 Summary of optimised & smoothed FoM values

Table 3 lists the final FoM results for all the algorithms with all the neutron fields used in the study.

Table 3. Optimised FoM values for each algorithm for the three data sets studied.

Source	Charge comparison	PGA	Model Pulse
^{241}Am/Be	1.13	1.10	0.93
5 MeV	1.35	0.91	0.98
^{252}Cf	1.38	1.01	0.93

The Charge Comparison algorithm has the most favourable figure, by a modest margin, in each of the cases. The model shapes for the Model Pulse algorithm were derived from the ^{241}Am/Be data, but its FoM is similar for all three data sets, indicating that the pulse shapes do not depend on the source of the neutrons and gammas.

5.5 Energy resolution

Figure 30 shows the light output spectrum from neutron events, derived from the 5 MeV monoenergetic data using the Charge Comparison algorithm. A corresponding spectrum from an analogue system [12], using a detector of the same dimensions, is overlaid. It is evident that the energy resolution of the two systems is very similar. (For the analogue system, the resolution at the light output of the recoil edge was determined [13] to be approximately 9%, in terms of the FWHM of the smearing Gaussian.)

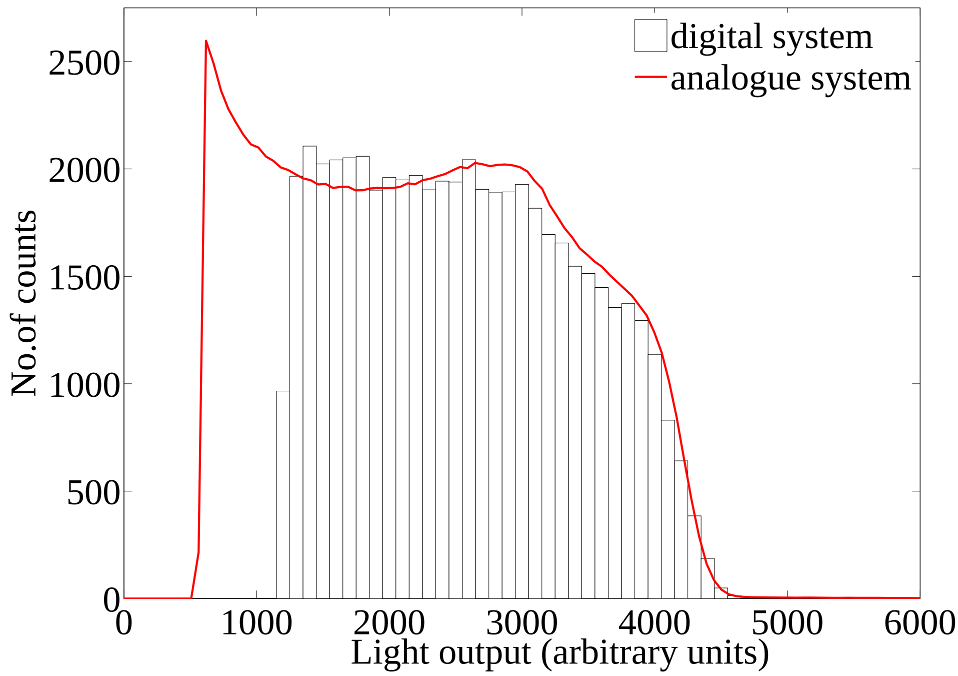

Figure 30. Light output spectra from 5 MeV monoenergetic neutrons.
Spectrum from the digital system, with the spectrum from an analogue system overlaid. The horizontal axis of the analogue spectrum has been scaled so that the recoil edges coincide, and the vertical axis scaled to match the area of the digital spectrum above the software threshold.

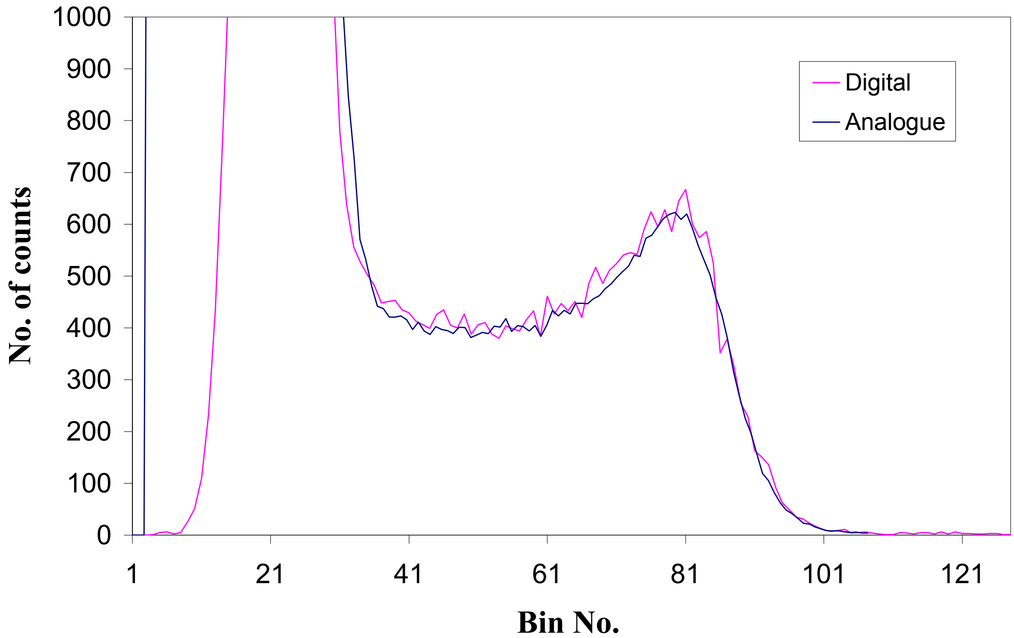

Figure 31. Light output spectra from ^{22}Na gamma source.
Comparison of spectra obtained using digital and analogue electronics with the same detector. The horizontal axis of the analogue spectrum has been scaled so that the Compton edges coincide, and the vertical axis scaled so that the peaks are the same height.

A similar comparison was carried out using a ^{22}Na gamma source (Figure 31). As no neutron / gamma discrimination was needed, the specialised photomultiplier base normally required for use with the analogue electronics of the Ref. [12] system was not necessary, so the same detector was used with both digital and analogue systems. The resolutions of the two spectra were again very similar, being approximately 12% for both (in terms of the 7/8 - 1/8 width of the 1.062 MeV Compton edge).

6 Conclusions

The Charge Comparison algorithm has a small but definite advantage in terms of FoM over the other two for the three neutron fields studied. It is also the simplest of the three, and (as implemented here) its long integral additionally serves as the total light output of the event.

The FoM for the other algorithms was not very much smaller, and each has advantages of its own. With the PGA algorithm used in real time, a decision on the type of event (neutron or gamma) is potentially available before the end of the pulse, provided the smoothing can be done as the samples are taken. The Model Pulse algorithm has the advantage that a piled-up or otherwise distorted pulse would show up readily as one in which both χ^2 values were very poor. However, if one wishes to implement real-time processing in a portable system where computing power is at a premium, the simplicity and good performance of the Charge Comparison method make it a strong candidate.

The digital system was found to be easy to set up, because of the small number of interconnections and controls. The contrast with the analogue system of Ref. [12] was significant.

The results with the neutron and gamma light output spectra show that the energy resolution of the digital system is comparable to that of the analogue system, making it suitable for dosimetric applications.

In future work it would be desirable to implement the Charge Comparison algorithm as embedded code in the FPGA (preferably including code for rejecting piled-up pulses), and to extend the study of the digital system to lower amplitude thresholds and higher gains. The apparent non-linearity and measurement artefacts seen in Figures 9 and 12 need to be investigated.

Acknowledgement

The authors are grateful to the National Measurement Office for financial support via the National Measurement System, and to the UK Department for Business, Innovation and Skills for their support via the Measurements for Innovators programme.

References

1 Saint-Gobain Crystals, *BC501A Data Sheet*, 2008.

2 J.M. Adams and G. White, *A versatile pulse shape discriminator for charged particle separation and its application to fast neutron time-of-flight spectroscopy*, Nucl. Instrum. Methods in Phys. Res. **156** (1978), 459 - 476.

3 R.B. Owen, Nucleonics **17** No. 9 (1959), 92.

4 S. Marrone, D. Cano-Ott, N. Colonna, C. Domingo, F. Gramegna, E.M. Gonzalez, F. Gunsing, M. Heil, F. Käppeler, P.F. Mastinu, P.M. Milazzo, T. Papaevangelou, P. Pavlopoulos, R. Plag, R. Reifarth, G. Tagliente, J.L. Tain and K. Wisshak, *Pulse shape analysis of liquid scintillators for neutron studies*, Nucl. Instrum. Methods in Phys. Res. **A490** (2002), 299 - 307.

5 D. Marocco, M. Riva, B. Esposito, L. Bertalot and A. Zimbal, *A digital data acquisition system optimized for spectrometry with liquid scintillation detectors*. In: International Workshop on Fast Neutron Detectors, Cape Town, 2006. Proceedings of Science (http://pos.sissa.it).

6 M.D. Aspinall, B. D'Mellow, R.O. Mackin, M.J. Joyce, N.P. Hawkes, D.J. Thomas, Z. Jarrah, A.J. Peyton, P.J. Nolan and A.J. Boston, *Verification of the digital discrimination of neutrons and gamma rays using pulse gradient analysis by digital measurement of time of flight*, Nucl. Instrum. Methods in Phys. Res. **A583** (2007), 432 - 438.

7 S.A. Pozzi, S.D. Clarke, M. Flaska and P. Peerani, *Pulse-height distributions of neutron and gamma rays from plutonium-oxide samples*, Nucl. Instrum. Methods in Phys. Res. **A608** (2009), 310 - 315.

8 Hybrid Instruments, *TOM Discriminator Data Sheet*, 2008.

9 M.J. Joyce, M.D. Aspinall, F.D. Cave, K. Georgopoulos and Z. Jarrah, *The design, build and test of a digital analyser for mixed radiation fields*. In: ANIMMA International Conference, Marseille, France, June 2009.

10 B. D'Mellow, M.D. Aspinall, R.O. Mackin, M.J. Joyce and A.J. Peyton, *Digital discrimination of neutrons and gamma-rays in liquid scintillators using pulse gradient analysis*, Nucl. Instrum. Methods in Phys. Res. **A578** (2007), 191 - 197.

11 C. Guerrero, D. Canno-Ott, M. Fernández-Ordóñez, E. González-Romero, T. Martínez and D. Villamarín, *Analysis of the BC501A neutron detector signals using the true pulse shape*, Nucl. Instrum. Methods in Phys. Res. **A597** (2008), 212 - 218.

12 S. Green, M. Scott and R. Koohi-Fayegh, *A users' guide for the NPL NE-213 Neutron Spectrometry System*, School of Physics and Space Research, University of Birmingham, September 1991, unpublished.

13 N.P. Hawkes and S.F Ashley, *Progress in Characterising the Neutron and Gamma Responses of the NPL Liquid Scintillation Spectrometers*, NPL Report IR 9, May 2008.